

Finite volumes vs finite elements. There is a choice

Ismet Demirdžić*

Department of Mechanical Engineering, University of Sarajevo, Sarajevo, 71000, Bosnia and Herzegovina

(Received December 18, 2019, Revised December 26, 2019, Accepted December 27, 2019)

Abstract. Despite a widely-held belief that the finite element method is **the** method for the solution of solid mechanics problems, which has for 30 years dissuaded solid mechanics scientists from paying any attention to the finite volume method, it is argued that finite volume methods can be a viable alternative. It is shown that it is simple to understand and implement, strongly conservative, memory efficient, and directly applicable to nonlinear problems. A number of examples are presented and, when available, comparison with finite element methods is made, showing that finite volume methods can be not only equal to, but outperform finite element methods for many applications.

Keywords: solid mechanics; finite volume method; finite element method; fluid-solid interaction

1. Introduction

Turner *et al.* (1956) published the paper that is considered as the start of the Finite Element Method (FEM), although the name was first used by Clough (1960). Since then, backed by the financial might of Boeing and NASA in the US and Rolls Royce in the UK and a rapid development and availability of electronic computers, FEM have undergone a phenomenal growth¹. Following a distinctive path, the Finite Volume Method (FVM) established itself as the leader in the field of fluid mechanics. While the FEM has been applied to fluid mechanics problems from early days of its development, e.g., Zienkiewicz *et al.* (1967), this ‘finite-element tsunami’ (Spalding 2006) has created ‘demonstrably false but widely-held belief that the FEM must be used for solid-stress problems and has wrongly dissuaded the majority of stress analysis researchers from paying any attention at all to FVM’ (Spalding 2008).

This might be a reason why there has been virtually no effort at developing FVMs for solid mechanics for 30 years. The first publication appeared in 1988 (Demirdžić *et al.* 1988), followed few years later by Beale and Elias (1991), Spalding (1993), Demirdžić and Martinović (1993), Demirdžić and Muzaferija (1994). All those methods, later named cell-centred FVMs, stem from the FVM for fluids and are developed without any reference to the FEM.

*Corresponding author, Professor, E-mail: i.demirdzic@yahoo.com

¹In 1965, NASA funded a project lead by Dick MacNeal to develop a more capable FEA software program and this became the program NASTRAN. This program cost \$3,000,000 to develop which is close to \$30,000,000 in today’s dollars (Tipton 2017).

Unaware of this original development, in the conference paper “Finite Volumes vs Finite Elements. Is there really a Choice?” (Zienkiewicz and Oñate 1991) and in its later journal version (Oñate *et al.* 1994) Zienkiewicz *et al.* stated that ‘the FVM can be considered to be a particular case of finite elements with a non-Galerkin weighting’ and that ‘the finite volumes are well known to be less accurate than Galerkin-based finite elements for self-adjoint (elliptic) problems’ because ‘Galerkin weighting provides an optimal approximation and must be more accurate than any alternative’. While these statements are by themselves true, they give impression that the FVM is a ‘poor relative’ of the FEM and by no means reflect the actual differences between the two methods. Namely, the FVM considered in those publications differs from the Bubnov-Galerkin FEMs only in setting the weighting function to unity instead of being equal to the element shape functions. It is called e.g., control-volume based FEM (Baliga and Patankar 1979, Voller 2009) or vertex-based FVM (Taylor *et al.* 2003). This uncertainty about the name reflects the method’s ‘hybrid’ nature and its applications demonstrate researchers’ reluctance to completely break the ties with FEMs, e.g., Fryer *et al.* (1991), Bailey and Cross (1995), Taylor *et al.* (2003).

However, although underfunded and underestimated, the cell-centred FVM of Demirdžić *et al.* (1988) have been extended to deal with: (i) more complex geometries (Demirdžić and Muzaferija 1994, 1995, Tuković *et al.* 2013), (ii) fluid-solid (Demirdžić and Muzaferija 1995, Kanyanta *et al.* 2009, Tuković *et al.* 2018) and structure-electrostatic (Das *et al.* 2011) interaction, (iii) various non-elastic (Demirdžić and Martinović 1993, Bijelonja *et al.* 2005, Tang *et al.* 2015) and anisotropic (Fainberg and Leister 1996, Demirdžić *et al.* 2000, Cardiff *et al.* 2014) materials, (iv) finite strains (Bijelonja *et al.* 2005, Tuković and Jasak 2007, Cardiff *et al.* 2014), (v) stresses and deformations during metal forming (Bašić *et al.* 2005, Lou *et al.* 2008, Cardiff *et al.* 2016b), wood drying (Martinović *et al.* 2001), phase-change (Teskeredžić *et al.* 2002) and casting (Teskeredžić *et al.* 2015a, b) processes, (vi) fracture mechanics (Ivanković *et al.* 1994, Stylianou and Ivanković 2002a, b, Carolan *et al.* 2013) and contact mechanics (Jasak and Weller 2000, Cardiff *et al.* 2012), (vii) modelling of beams (Fallah and Hatami 2006, Isić *et al.* 2007), plates (Demirdžić and Ivanković 1997, Das *et al.* 2012, Fallah and Parayandeh-Shahrestany 2014), and shells (Hatami *et al.* 2006).

Impressive reductions in CPU times were obtained when (i) multigrid methods (Fainberg and Leister 1996, Demirdžić *et al.* 1997, Ivanković *et al.* 1997), (ii) fully coupled solution algorithms (Das *et al.* 2011, Cardiff *et al.* 2016a) or (iii) massively parallel processing (Demirdžić 2008, Cardiff *et al.* 2018) were employed.

It has been established that up to date more than 500 journal and conference papers, 40 PhD theses, and four books dealing with various flavours of the finite volume methods for solid mechanics, including ‘cell-centred’, ‘vertex-centred’, ‘staggered’, ‘Godunov-type’, ‘meshless’, as well as others have been published (Cardiff and Demirdžić 2018).

Within this article, the FVM stands for the cell-centred approach originally proposed by Demirdžić *et al.* (1988) and later extended by a number of authors, while the FEM refers to the continuous Bubnov-Galerkin method as described, for example, in Bathe (1996).

In what follows the mathematical models employed by FVM and FEM are briefly presented. This is followed by highlighting the similarities and differences between these two methods and their relative advantages and disadvantages. After that, the ways of improving the efficiency, the main disadvantage of the FVM, are discussed. Finally, a number of examples of application of FVM and comparison with FEM are given.

2. Mathematical model

2.1 Governing equations

The FVM is based on the conservation of momentum principle, i.e., on the balance of (surface and body) forces applied to the finite control volume V bounded by the surface S with the outward pointing vector \mathbf{s} , resulting in the so-called ‘strong conservation form’

$$\int_V \rho \frac{\partial^2 \mathbf{u}}{\partial t^2} dV = \int_S \boldsymbol{\sigma} \cdot \mathbf{w} dV + \int_V \rho \mathbf{f}_b dV \quad (1)$$

where t is the time, ρ is the density, \mathbf{u} is the displacement, $\boldsymbol{\sigma}$ is the Cauchy stress tensor, and \mathbf{f}_b is the body force. The FEM applies the Gauss theorem to the surface integral in (1) and then uses the principle of virtual work or the method of weighting residuals to obtain the so-called ‘weak conservation form’

$$\int_V \rho \frac{\partial^2 \mathbf{u}}{\partial t^2} \cdot \mathbf{w} dV = \int_S \text{div } \boldsymbol{\sigma} \cdot \mathbf{w} dV + \int_V \rho \mathbf{f}_b \cdot \mathbf{w} dV \quad (2)$$

or in a more familiar form, obtained after some rearrangement of the first term on the right end side

$$\int_V \rho \frac{\partial^2 \mathbf{u}}{\partial t^2} \cdot \mathbf{w} dV = - \int_V \boldsymbol{\sigma} : \text{grad } \mathbf{w} dV + \int_V \rho \mathbf{f}_b \cdot \mathbf{w} dV + \int_S \mathbf{w} \cdot \boldsymbol{\sigma} \cdot d\mathbf{s} \quad (3)$$

where \mathbf{w} is the virtual displacement or the weighting function. It is obvious that (2) can be viewed as a generalisation of (1) or (1) as a special case of (2), obtained by setting $\mathbf{w}=\mathbf{1}$.

2.2 Constitutive relations

After 60 years of countless man-hours and generous financial support it is not surprising that the present day FEMs include a wide range of constitutive relations for metallic and non-metallic, linear and materially and geometrically non-linear materials, see e.g., Abaqus Theory Manual (2012). Apart from the constitutive relation for the standard linear (Hookean) elastic body, a number of other constitutive relations have been used in FVMs. For example, the OpenFOAM offers the following constitutive laws for linear geometry: thermo-linear elastic, orthotropic linear elastic, linear visco-elastic, poro-linear elastic, Mises/J2 plastic, Mohr-Coulomb plastic, as well as for non-linear geometry: Neo- Hookean elastic, St. Venant Kirchhoff elastic, orthotropic St. Venant Kirchhoff elastic, Neo-Hookean elastic, Mises/J2 plastic (Cardiff *et al.* 2018).

3. Finite volumes vs finite elements

To explain similarities and differences between FVM and FEM, let us recall that all numerical methods consist of the following main components:

- (a) discretisation of time and space,
- (b) discretisation of the equations of the mathematical model, and
- (c) solution algorithm

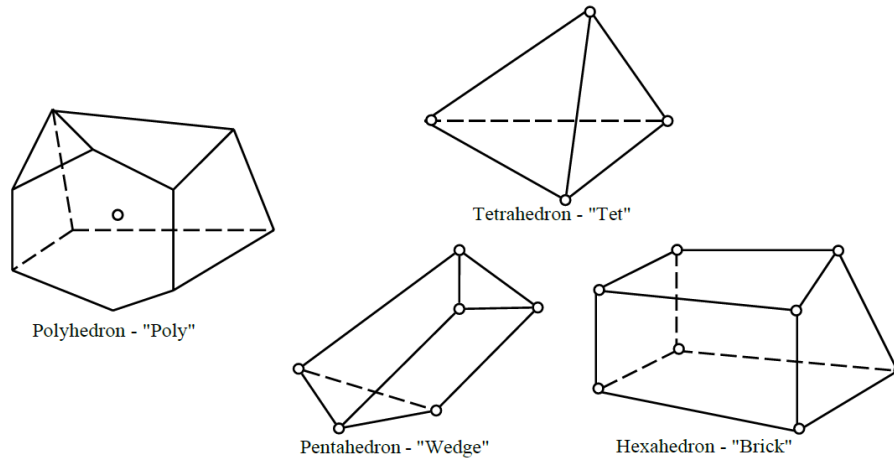


Fig. 1 Arbitrary polyhedral control volume (left) and standard finite elements (right)

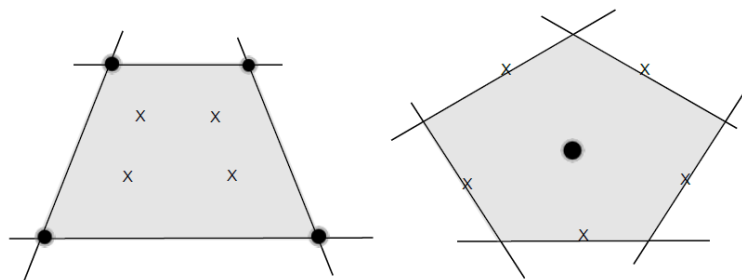


Fig. 2 2D element (left) and control volume (right). • – nodes, x – integration points

(a) Both FEMs and FVMs subdivide the time into a number of time steps and the spatial solution domain into finite nonoverlapping subdomains called *elements* in the FEM terminology and *control volumes* or *cells* in the FVM terminology. Elements are typically tetrahedra, wedges or hexahedra. Control volumes (CVs) are of arbitrary polyhedral shape (Fig. 1) and all polyhedra (e.g., tetrahedra, hexahedra, triangular prism, dodecahedra, etc.) are discretised in the same manner. This is in contrast to the FEM, where the number of shapes of the elements is limited, the shape functions are specific to the shape of the element, and mesh conformity is necessary, i.e., hanging nodes need to be handled to avoid non-conforming discretisations.

(b) In the FEM the displacements are evaluated at the nodes-points situated at the corners (and along the edges) of the elements, while the stresses are evaluated at the Gauss points using only one element and the shape functions of that element to calculate the displacement gradients. In the FVM the displacements are known at the cell centers and the neighbour cell displacements and the Gauss theorem or the least square method are used to obtain gradients at the cell centers which are then interpolated to the cell-face centers and used to calculate the cell-face stresses (Fig. 2). It is important to note that the FVM discretisation leads to the conservation of momentum on the local, CV level and consequently on the whole solution domain, while the FEM is only globally conservative.

(c) The major discriminating factor between the FEM and the FVM is the discrete equations are actually solved. FVMs use segregated solution algorithm, like the ones found in Computational Fluid Dynamics, which linearises and (temporarily) decouples equations for individual displacement

Table 1 Solution strategies of FEM and FVM.

Method	Solution algorithm	Lin. equ. solver	Main features
FEM	Fully coupled	Direct	Fast, stable; memory 'hungry'
FVM	Segregated	Iterative	Very low memory, conservative; slow convergence

component in such a way that the stiffness/coefficient matrix contains only the contribution from the nearest neighbours of each cell even though the actual 'stencil' of cells can be much larger, resulting in a very sparse diagonally dominant coefficient matrix. This enables the resulting set of linear algebraic equations to be easily solved by a number of iterative (typically conjugate gradient or algebraic multigrid) solvers which retain the sparsity of the matrix (no fill-in!). Since the coefficients and sources are only approximate (based on the values of displacements and physical parameters from the previous iteration) the linear solver does not need to converge to a tight tolerance, but only sufficiently to provide a reasonably 'smooth' solution and a reduction in the residuals of one or two orders of magnitude is typically sufficient. Outer Picard/Fixed-Point iterations are employed to account for the inter-equation coupling and the linearised nonlinear terms. They are performed until a predefined tolerance, typically 1×10^{-6} , is achieved.

The FEM discretisation results in a relatively densely populated coefficient matrix² requiring a direct linear algebraic equation solver which additionally fills-up the coefficient matrix. The direct solvers are robust and are less sensitive to the quality of the grid. But nonetheless, typically the CPU and memory costs are almost quadratic functions of the number of nodes. This means that much of the memory needed for problems with large degrees of freedom (DOF) must be stored on the disk rather than RAM. While the FVM solution procedure for non-linear problems remains essentially the same as for linear ones, FEMs typically use a full or modified Newton-Raphson loop to resolve nonlinearities which, in contrast to Picard iterations, necessitates the need for a consistent tangent matrix for optimal convergence (Bathe 1996). The Newton method can achieve quadratic convergence compared with the linear convergence rate of the Picard iterations. However, each Newton iteration is much more expensive; it practically repeats all calculations at each iteration, while the FVM resolves (material) nonlinearities 'on the fly' at each iteration, with no or little additional cost compared to linear problems.

The most common FEM and FVM solution strategies are summarised in Table 1. As can be seen, the relative weakness of the FEMs is large memory requirement, while the main deficiency of the FVMs can be a slow convergence, most notably in case of strong inter-component coupling, resulting in prohibitive CPU times, both weaknesses steaming from the adopted solution strategies.

A number of ways have been developed to reduce the FEM memory requirements, e.g., banded stiffness matrices or iterative solvers which require considerably less storage than direct solvers, but are not guaranteed to converge. These issues will not be further discussed here. Instead, the ways to alleviate the FVMs deficiency will be presented in the next Section.

4. Enhancing FVM efficiency

The FVM is extremely memory efficient (the memory is essentially linear with the number of

²For a numerical mesh made of N hexahedral CVs/bricks the FVM requires $7N$ and the FEM $243N$ coefficient matrix entries.

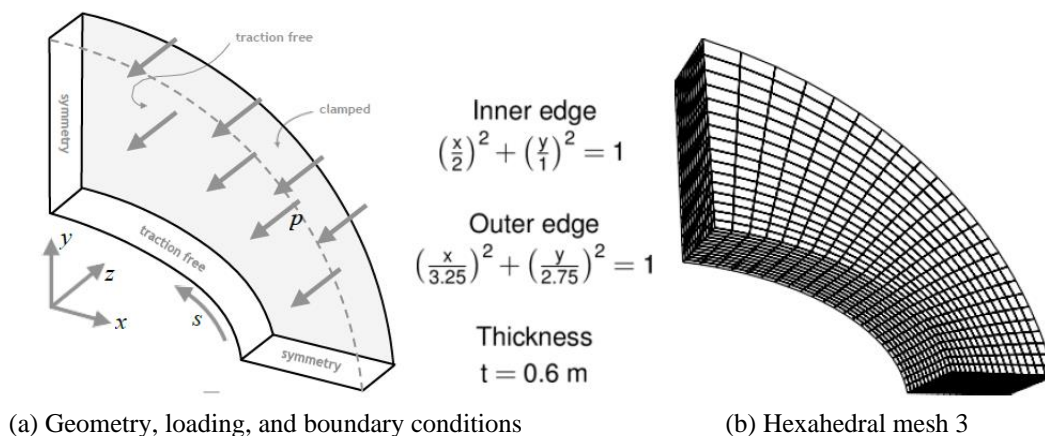


Fig. 3 Out-of-plane bending of an elliptic plate (Cardiff *et al.* 2016a)

DOF). It requires up to 1000 times less memory than the typical FEM direct solvers and about 10 times less memory than iterative FEM solvers with the same number of DOF, but can suffer from a poor convergence when the inter-displacement-component coupling is strong. To overcome this inadequacy, several procedures are proposed. The major reductions of the CPU time are obtained by applying the geometric multigrid or block-coupled solution methods. A modest improvement, but with much less programming effort, is achieved by employing the convergence acceleration (Aitken's and based on estimation of iteration errors). Finally, a massively parallel processing usually achieves a linear speedup and enables an efficient solution of very large problems.

Where available, comparisons with FEM results are made.

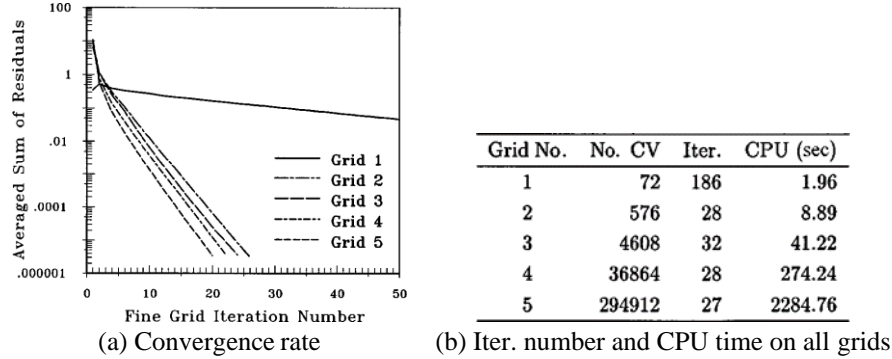
4.1 Multigrid method

An early attempt to tackle the slow convergence problem is made by Demirdžić *et al.* (1997). They applied a full multigrid method to a thick elliptic plate with a centred elliptic hole, fully clamped at the outside edges and loaded by a constant pressure of 1 MPa at the upper surface (the NAFEMS Standard Benchmark Test LE10 (NAFEMS 1990)), Fig. 3. Due to a double symmetry, only a quarter of the plate is taken for the solution domain. Calculations were performed in double-precision on a IBM RISC System 6000/530 workstation, with PowerPC processors running at 25 MHz using five systematically refined grids ranging between 72 and 294,912 CVs.

Fig. 4 shows the asymptotic convergence rate and respectable computing times of the full multigrid solution method. The number of fine grid iterations is almost constant and the CPU time is proportional to the number of computational points. The times shown correspond to the convergence tolerance of 10^{-5} , which corresponds to the accuracy to within four to five significant digits. However, for most practical applications discretisation errors of the order of 1% are acceptable and the convergence tolerance of 10^{-3} would suffice; the number of required iterations and computing time are much lower in this case, as shown in Table 2.

4.2 Block-coupled FVM

In order to improve efficiency of the FVM the block-coupled solution methods are developed,

Fig. 4 Convergence properties for the elliptic plate problem (Demirdžić *et al.* 1997)Table 2 Memory and CPU times necessary to obtain converged solution on all grid levels using double precision arithmetic on an IBM RISC System 6000/530 workstation (Demirdžić *et al.* 1997)

No. CVs	No. deg. freedom	No. grid levels	Memory (MB)	Sol.tol. 10^{-5}		Sol.tol. 10^{-3}	
				Fine grid iter.	CPU (min)	Fine grid iter.	CPU (min)
294 912	884 736	5	148.19	27	38.1	16	22.6

where inter-component coupling is implicitly included as coefficients in a block matrix (Das *et al.* 2011, Cardiff *et al.* 2016a). It has been found that the coupled method is faster than the segregated FVM with approximate speed-ups ranging from 5 times for problems with weak inter-component coupling to three orders of magnitude for problems with very strong inter-component coupling (e.g., the bending of a 2-D slender cantilever). As expected, the coupled method required approximately 4 times more memory than the segregated methods. When compared with FEMs, the coupled method has been found to be more efficient in terms of both CPU time and memory than low order FEMs.

4.2.1 Out-of-plane bending of elliptic plate

Cardiff *et al.* (2016a) used the NAFEMS Benchmark LE10 case (NAFEMS 1990) (Fig. 3) to compare performances of segregated and coupled FVM and commercial FE software Abaqus (version 6.11-1 - reduced integration, bi-linear quadrilaterals) (Abaqus Theory Manual 2012). They performed calculations on the same set of five hexahedral meshes as Demirdžić *et al.* (1997). The segregated FVM employs a CG method with incomplete Cholesky preconditioning and the coupled FVM uses BiCGStab linear solver with ILU(0) preconditioner, both with the tolerance of 1×10^{-6} , while Abaqus employs a direct solver.

The stress contours in the $z=0.3$ m x - y plane are shown in Fig. 5, comparing the FVM solutions obtained on the finest hexahedral mesh and on the polyhedral 275,533 CV mesh with the Abaqus solution and with the Demirdžić *et al.* (1997) benchmark. All results are seen to agree closely.

The execution times and memory for segregated FVM are compared with the coupled FVM and with Abaqus in Table 3. It can be seen that the coupled FVM is 2.5 to 6 times faster than the segregated FVM method and, as expected, the memory requirements of the coupled FVM are greater, by approximately 4.5 times in the largest mesh case. Interestingly, when compared to the FE solution, the coupled method is faster and considerably more memory efficient in all cases. The larger memory requirements of the FE solution may be attributed to the employed direct solver.

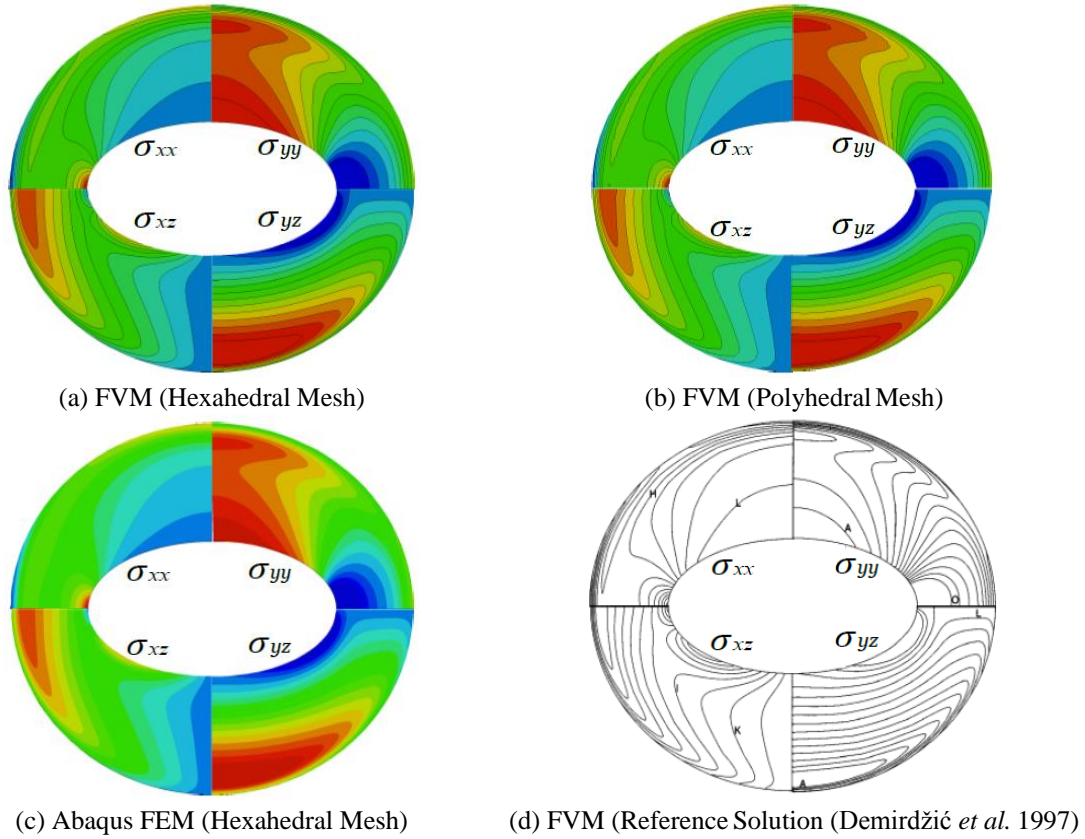


Fig. 5 Elliptic plate: stress component distributions on the plane $z = 0.3$ m for FVM hexahedral and polyhedral mesh and the Abaqus FE hexahedral mesh solution (Cardiff *et al.* 2016a)

Table 3 Elliptic plate: wall-clock time (in s) and maximum memory usage (in MB) (Cardiff *et al.* 2016a)

Mesh	Segregated FVM		Coupled FVM		Abaqus FEM	
	Time	Memory	Time	Memory	Time	Memory
72	0.5	6	0.03	7	4	24
576	1	8	0.15	13	5	31
4 608	6.5	20	1.6	51	6	107
36 864	102	80	11	300	34	1 197
294 912	1 474	500	242	2 200	1 375	17 900

4.2.2 Slender cantilever in bending

A rectangular elastic beam with the Young's modulus 200 GPa and the Poisson's ratio 0.3, with length to height ratio of 20:1 is fixed at one end and loaded by uniformly distributed traction of 0.1 MPa at the other end. It should be noted that this test case is a *worst case scenario* for a segregated approach, due to the dominant inter-component coupling.

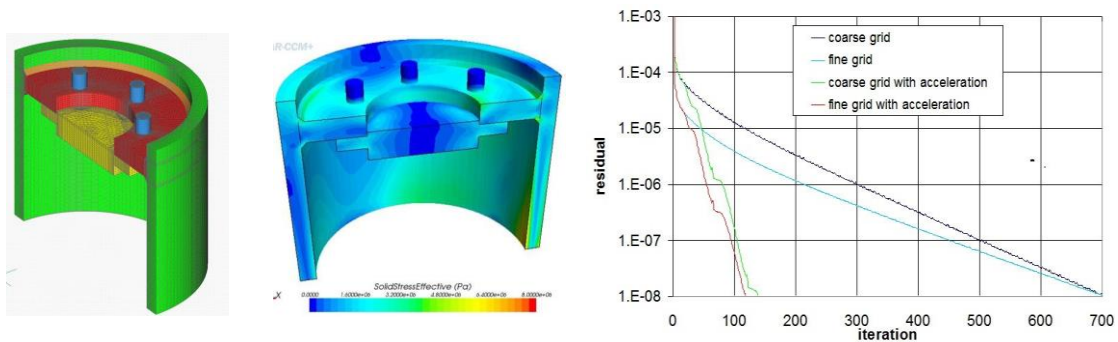
Five uniform quadrilateral meshes are employed. The models are solved in double precision using 1 CPU core (2.4 GHz Intel Ivy Bridge cores). The segregated FVM employs a CG method

Table 4 Slender cantilever: wall-clock time (in s) and maximum memory usage (in MB) (Cardiff *et al.* 2016a)

Mesh	Segregated FVM		Coupled FVM		Abaqus FEM	
	Time	Memory	Time	Memory	Time	Memory
500	58	20	0.08	11	3	40
4 500	384	27	0.5	50	4	113
12 500	1 387	43	1.4	140	5	197
50 000	4 737	112	6	570	16	881
200 000	--	--	36	2 500	73	1 800

Table 5 Wheel model: CPU and memory comparisons to FEM for elastic wheel (Demirdžić 2008)

Grid	CPU (min)		Memory (Mb)	
	FVM	Abaqus FEM	FVM	Abaqus FEM
Coarse (30 000 cells)	2.1	1.0	41	615
Fine (245 000 cells)	19	49	307	6 500 (out of core!)



(a) Rim, disk, weldments, bolts and numerical mesh

(b) Effective stress

(c) Convergence rate with and without acceleration for coarse and fine grid

Fig. 6 Wheel model (Demirdžić 2008)

with incomplete Cholesky preconditioning and a relatively tight solution tolerance of 10^{-8} , while coupled FVM and FEM use direct solvers.

Table 4 shows the wall-clock times and memory requirements for each of the runs. It can be seen that the segregated FVM is very memory efficient, but is hopelessly slow. When comparing the coupled FVM and FEM, the coupled FVM is at least twice as fast and requires slightly less memory.

4.3 Convergence acceleration

Several other ways of tackling slow convergence of the FVM fixed point iterations were employed; among them González *et al.* (2018) employed Aitken acceleration and Perić (2004) used acceleration based on iteration error estimate. They both applied them to NAFEMS LE10 case (NAFEMS 1990) (Fig. 3) and obtained speed-ups of 4.3 and 3.5, respectively, and to a slender cantilever with speed-ups of 5.5 and 10, respectively.

In addition to the above academic cases, Demirdžić (2008) applied acceleration based on iteration

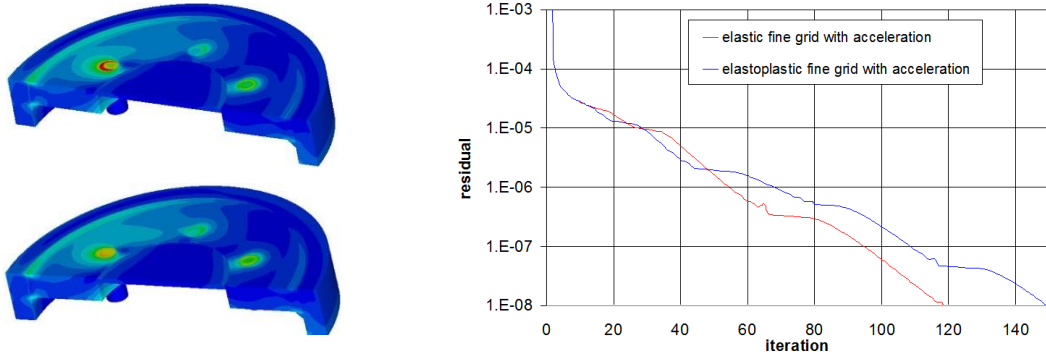


Fig. 7 Wheel model: effective stress on plane between disk and shaft for elastic (top left) and elastoplastic (bottom left) material and convergence rate (right) (Demirdžić 2008)

error estimate to analyse a wheel model with rim, disk, weldments, bolts, and shaft made of a linear elastic material shown in Fig. 6(a). Two mostly hexahedra-cell grids are employed: coarse with 30,000 cells and fine with 245,000 cells. Fig. 6(c) shows that the problem converges in about the same number of iterations for both the coarse and the fine grid. It can also be seen that the acceleration based on the iteration error estimate significantly reduces the number of iterations for both grids.

Comparisons are made to the FE commercial code Abaqus (Abaqus Theory Manual 2012). Both the FVM and the FEM code were run on Linux/x86-32 on x86-64 single processor Intel Xeon with 2 Gb RAM, 3.2 GHZ computer and both codes predict almost identical results on identical mesh. Table 5 shows comparison of FVM and FEM regarding CPU time and memory for coarse and fine mesh. Typically, in case of the coarse mesh FEM is faster (two times), but requires more memory (15 times), while in the case of fine mesh the direct FEM solver requires more memory than available on the RAM and it is outperformed by the FVM both in terms of CPU time and memory.

Finally, the results for the wheel made of an elastoplastic material are shown in Fig. 7 and compared with those for the elastic wheel. Since the FVM updates nonlinearity continuously after each iteration, the CPU time required to arrive at the solution for elastoplastic case is almost the same as for linear elastic one.

4.4 Parallel performance

While comparison of serial execution times and memory usage is beneficial, of increasing importance is the parallel performance of the methods, where the multiple CPU cores of a computer or a cluster are exploited. For standard finite volume and finite element procedures, the most time consuming component is the solution of the linear system of equations; as iterative linear solvers are better-suited to parallelisation than direct solvers, standard finite volume methods have been shown to provide better parallel scaling, ultimately allowing analysis of larger problems.

4.4.1 Heated spherical pressure vessel

An internally heated and pressurised hollow spherical vessel, Fig. 8, is assessed for parallel efficiency by Cardiff *et al.* (2018). The outer surface is specified as traction free, with a surface convective heat coefficient of $90 \text{ W/m}^2\text{K}$. The reference temperature is assumed to be 300 K. At the initial time the zero displacement and velocity and temperature of the 300 K in the whole solution domain are specified. The assumed thermo-mechanical material properties are given in Fig. 8 (right).

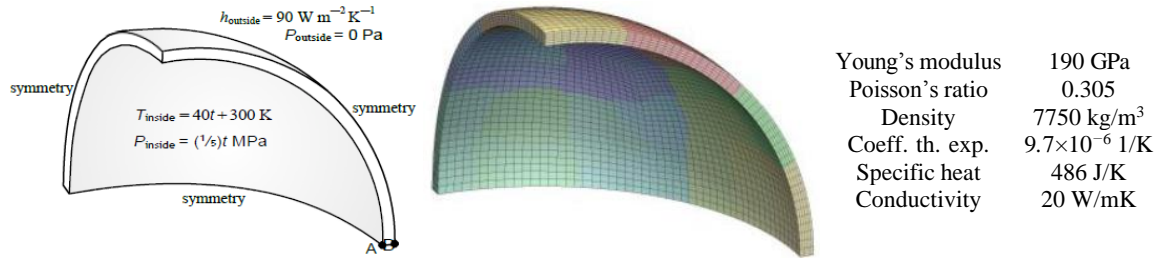
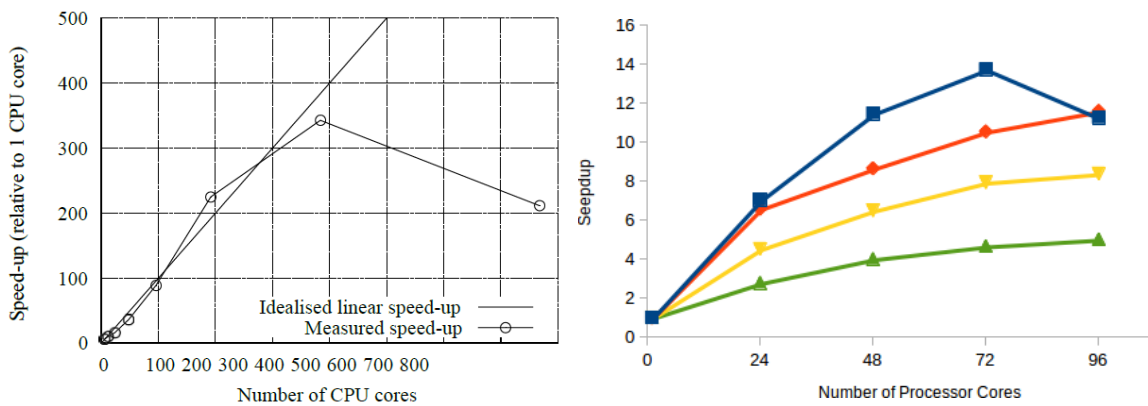


Fig. 8 Heated spherical pressure vessel: geometry and loading (left), mesh and domain decomposition (middle), and mechanical properties (right) (Cardiff *et al.* 2018)

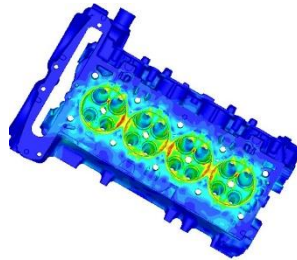


(a) FVM: Heated spherical vessel (Cardiff *et al.* 2018) (b) FEM: Abaqus benchmarks □-S2A, ◇-S4B, ▽-S4D, △-S6 (ICHEC 2013)

Fig. 9 Parallel performance of FVM and FEM

The spatial solution domain, a quarter of the sphere, is discretised by a 4.8 million CV hexahedral mesh and a constant time-step of 1 s that was found to produce time-step independent results is employed.

The problem is solved using increasing numbers of CPU cores varying from 6 to 768 CPU cores; the METIS decomposition method has been used to decompose the domain. The *Fionn* supercomputer from the Irish Centre for High-End Computing has been used for all calculations, where each computer node contains two Intel Xeon (E5-2660 v2 @ 2.20GHz, 25.6 MB of cache) CPUs and 64 GB of RAM. The solution for the finest mesh was achieved in under half an hour using 384 CPU cores, in comparison to over 150 hours when using 1 CPU core. The parallel speedup is shown in Fig. 9(a). It can be seen that the method scales in an approximately linear fashion up until 384 CPU cores. This corresponds to approximately 12 500 cells per CPU core. As the number of CPU cores are increased further to 768, the parallel efficiency drops. In contrast, the direct linear equation solvers, as used by FEMs, show a mediocre parallel scaling, as illustrated in Fig. 9(b) where the parallel performance of a number of Abaqus 6.13 benchmark cases (Abaqus Documentation 2013) is presented. Although this is not a direct comparison, all runs were made on the same hardware and do show typical behaviour of iterative and direct linear solvers. Iterative solvers hold the upper hand for parallelisation and consequently typical FVMs benefit from this. However, the use of iterative linear solvers with FEMs will no-doubt improve their parallel performance.



No of proc.	Cells per processor	CPU time (min)	Speed up
1	4.2 million	324	1
4	1.05 million	81.18	3.99
8	525 000	45.00	7.20
16	262 500	20.15	16.08
32	131 250	14.08	23.01

Fig. 10 Engine block and head: effective stress (left) and parallel scalability (right) (Demirdžić 2008)

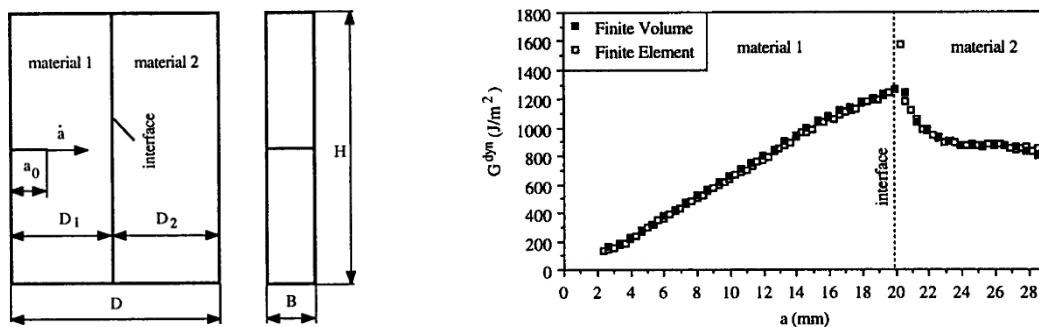


Fig. 11 Rapid crack propagation: duplex SENT geometry ($D_1=19.8$ mm, $D_2=9.3$ mm, $H=100$ mm, $a_0=2$ mm) (left) and crack driving force vs. crack length (right) (Ivanković *et al.* 1994)

4.4.2 Engine block and head

Another example of parallel performance is an industrially relevant case, calculation of thermal stresses in an engine block and head made of a thermoelastic material. The solution domain is discretised with 4.2 million cells (12.6 million DOFs) requiring 9.8 Gb RAM and run on a Cray node AMD opetron 250, 2.4 GHz, 4 Gb RAM per node, Rapid Array MPI computer. Calculated effective stress is shown in Fig. 10 (left) and the parallel performance is illustrated in Fig. 10 (right). A very good scalability is obtained to about 200,000 cells per processor and then departs from linear. However, less than 15 min to get an answer for a 4.2 million cell real-life model is an impressive result.

5. Examples of FVM applications

In what follows a number of applications of FVM to academic and industrially relevant cases will be presented and, when available, comparison with FEM will be made.

5.1 Small deformations of isotropic and orthotropic elastic bodies

5.1.1 Rapid crack propagation

One of the first FVM applications to solids was predictions of the rapid crack propagation in a duplex SENT sample, Fig. 11 (left) (Ivanković *et al.* 1994). The calculation began by a release of the crack tip cell face. The crack propagated at a constant speed $\dot{a}_1=344.3$ m/s in material 1 ($E_1=6$ GPa, $\nu_1=0.33$, $\rho_1=1180$ kg/m³), arrested at the interface for a short period ($t_{arrest}=1.2$ μ s), and continued

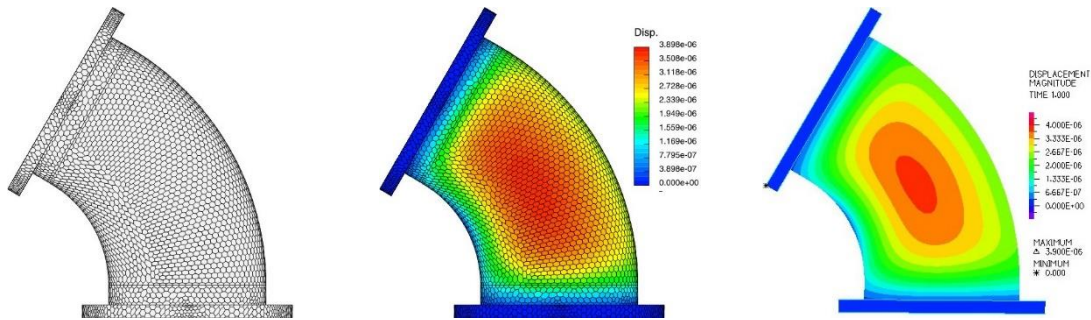


Fig. 12 Pipe elbow: computational mesh (left) and displacement magnitude calculated by FVM (middle) and ADINA FEM (right) (Bijelonja *et al.* 2017).

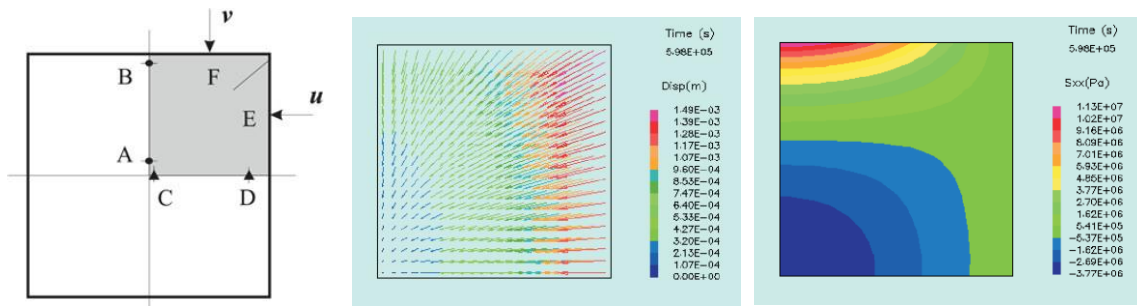


Fig. 13 Drying of a wood beam: solution domain and reference points (left) and displacement (middle) and normal stress (right) fields at $t=166$ h (Martinović *et al.* 2001)

with a lower constant speed $\dot{a}_2=265$ m/s through the material 2 ($E_2=3$ GPa, $\nu_2=0.39$, $\rho_2=1190$ kg/m³). During the computation the specimen is regarded as being under fixed grip conditions.

Fig. 11 (right) shows the comparison between the FVM and FEM dynamic energy release rate G^{dyn} results and very good agreement is demonstrated. The FVM results are obtained on a 2640 CV Cartesian mesh, while in the FEM solution a mesh consisting of constant strain triangular elements with 14,952 nodes were used, whereby the FEM required 11 times more computer memory than the FVM.

5.1.2 Pipe elbow under internal pressure

The stress and deformation analysis of a pipe elbow flanged at both ends is performed by Bijelonja *et al.* (2017) and the results are compared with those obtained using the commercial FE software ADINA (ADINA 2012).

The material of the elbow is assumed to be linear elastic with Young's modulus 2.1×10^5 MPa and Poisson's ratio 0.3. At the outer surfaces of both flanges zero displacements are assumed. The inner elbow surface is loaded by the pressure of 1 MPa. All other boundaries are considered stress free. The solution domain is discretised by a polyhedral mesh consisting of 20,744 CVs as shown in Fig. 12(left).

Fig. 12 (middle and right) shows the displacement magnitude field. A very good agreement between FVM and FEM solutions can be seen. The almost identical maximum displacement values located at the inner surface of the elbow at the middle of the flange span of 3.898×10^{-6} m for the finite-volume and 3.900×10^{-6} m for the finite-element solution are obtained.

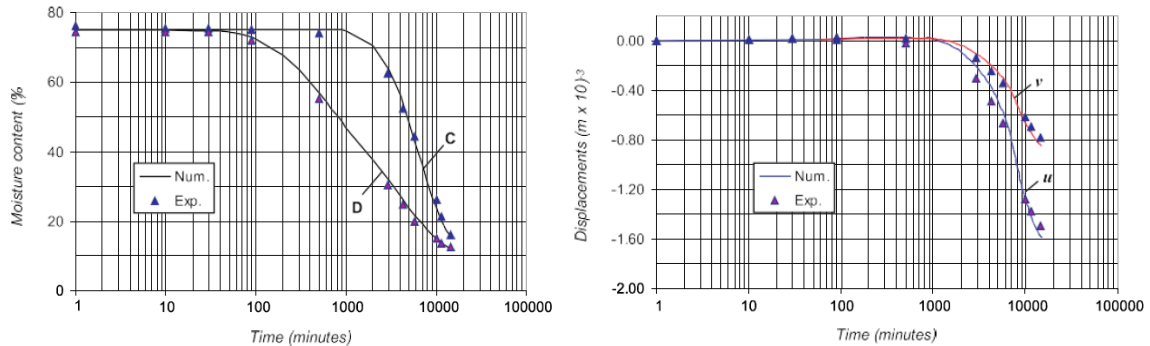


Fig. 14 Drying of a wood beam: moisture content at points C and D (left) and u displacement at point E and v displacement at point F (right) (Martinović *et al.* 2001)

5.1.3 Drying of a wood beam

Martinović *et al.* (2001) used the FVM to analyse a wood drying process, which is governed by the energy, mass and momentum balance equations. Beech-wood beams ($600 \times 50 \times 50$ mm) are exposed to the uniform, unsteady flow of hot air in a laboratory dryer. The beam material is considered to be elastic orthotropic and its temperature and/or moisture dependent physical properties are given in Martinović *et al.* (2001). The problem is considered to be a 2D plane strain. Due to the double symmetry only one quarter of the cross section is taken as the solution domain, as shown in Fig. 13(left).

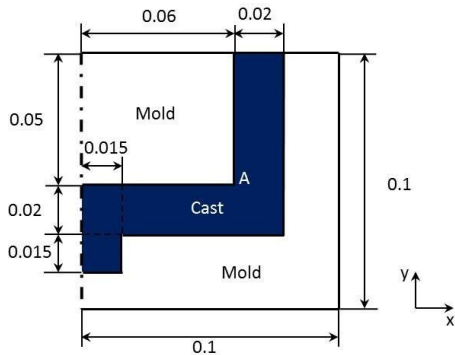
During the initial phase (first two hours) of drying the moisture content is above the fiber saturation point and the deformation is a consequence of the thermal stresses only. During the period of intensive drying (between 60 and 190 hours) the deformation and stresses due to hygral loads dominate. At $t=166$ h the moisture content has fallen below the fiber saturation point, and that this causes the shrinking of the wood sample, Fig. 13(center), and extensive stresses in the outer region and compressive stresses in the interior of the sample, Fig. 13(right).

Fig. 14 shows moisture content and displacements histories at two reference points shown in Fig. 13(left). One can see very little deformation during the initial phase ($t \leq 1000$ minutes) and a considerable shrinking of the sample afterwards, and that predictions closely follow experimental data.

5.2 Deformation and stresses in casting

Teskeredžić *et al.* (2002) analysed a casting problem using two material models, the Duhamel-Neumann form of the Hooke's law (TE solid) and the Perzyna model (TEVP solid). The problem geometry and the physical properties of the solidified cast and the mold are given in Fig. 15. It is assumed that the mold is completely filled with the solidified metal at the uniform temperature of 120°C which corresponds to the stress free condition and is higher than the initial temperature of the mold of 100°C . All solution domain boundaries are set to the constant temperature of 100°C . The friction between the cast and the mold is neglected and the influence on the heat transfer of the air gaps at places where no contact exists are accounted for.

A grid and time-step independent solution is obtained by employing the uniform 180×180 CV mesh and the time step of 1 s. The process is led in such a way that after 100 s of the real time in which the temperature within the calculation domain is uniform (tolerance ± 1 K) the mold is 'crashed' and



	Young mod. (Pa)	Yeald st. (Pa)	Pois. coef.	Th.exp.c. (1/K)
Cast	2.1×10^{11}	2.1×10^8	0.33	3.05×10^{-5}
Mold	—	—	—	—
	Conduct. (W/mK)	Density (kg/m ³)	Sp.heat (J/kgK)	
Cast	160	7800	460	
Mold	60	7800	460	

Fig. 15 Geometry of the cast-mold assembly (dimensions in m) (left) and physical properties for solidified cast and mold (right) (Teskeredžić *et al.* 2002)

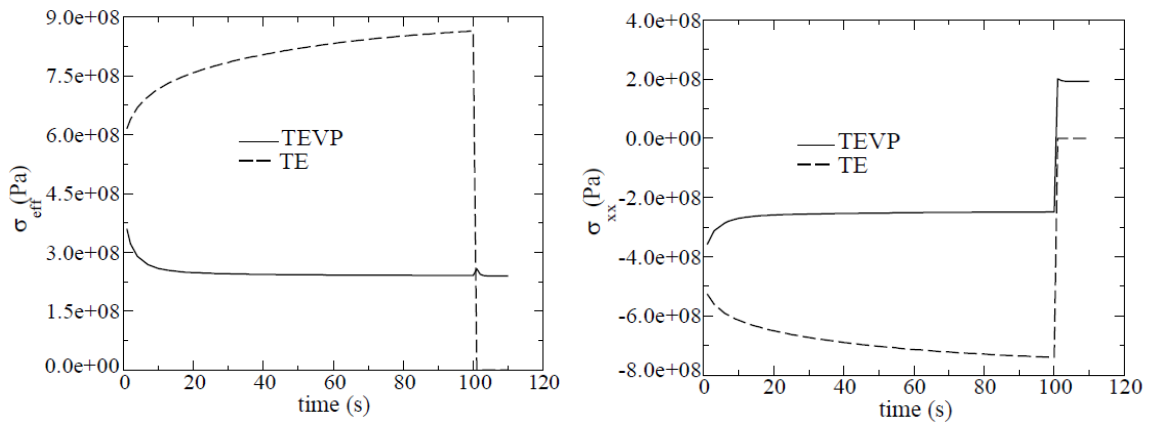


Fig. 16 Effective stress σ_{eff} (left) and normal stress σ_{xx} (right) for TEVP and TE models at point A in the corner of the cast; at $t=100$ s mold is ‘crashed’ (Teskeredžić *et al.* 2002)

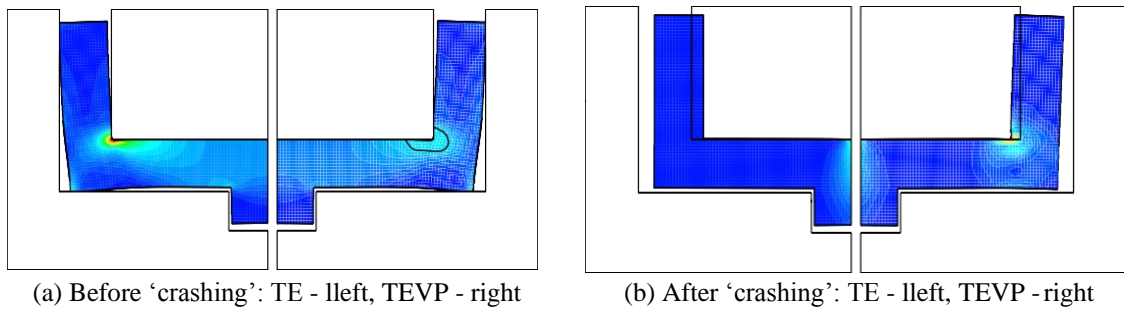


Fig. 17 Shape of the cast and effective (residual) stresses (Teskeredžić *et al.* 2002)

the whole force coming from the mold is applied to the cast within the next time increment and the solid is then let free to reach a new steady state. In Fig. 16 the effective and normal stresses are given for the point A in the corner of the cast where the stresses reach the maximum value. As can be seen, the stresses for the TE solid decrease to zero as soon as the contact force is removed, while in the TEVP solid the non-zero residual stresses remain.

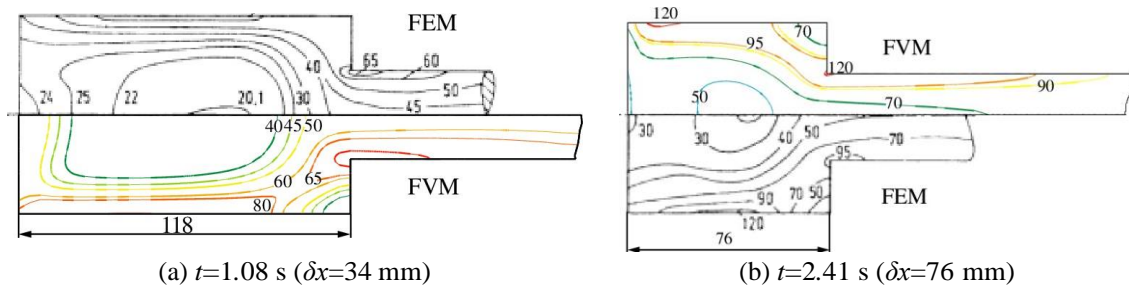


Fig. 18 Forward extrusion through axisymmetric die: temperature distribution (Bašić *et al.* 2005)

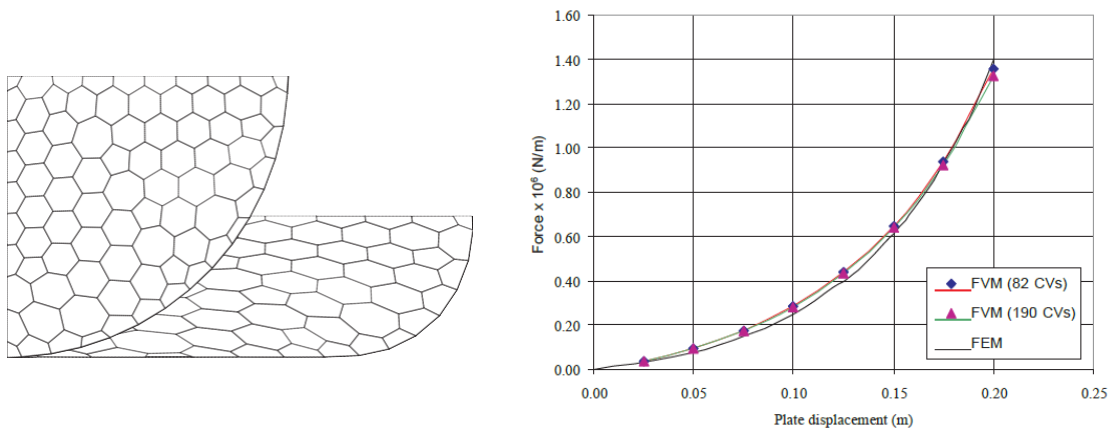


Fig. 19 Deformation of a rubber cylinder: initial and deformed (displacement of 0.2 m) mesh (left) and comparison of FVM and Ansys FEM (Ansys Verification Manual 2004) results (right) (Bijelonja *et al.* 2005)

Fig. 17 shows the cast shape and the effective stresses after the cast is cooled before and after the ‘crashing’ the mold, respectively. The black contour at the corner of the cast where the concentration of stresses is the highest, Fig. 17(a) (right), marks the position where the effective stress is equal to the yield stress and the residual stresses and deformations in that region are visible for TEVP solid, Fig. 17(b) (right), while in the TE solid they do not exist, Fig. 17(b) (left).

5.3 Large deformations of non-elastic bodies

Examples employing governing equations in arbitrary Lagrangian-Eulerian, total Lagrangian, and updated Lagrangian form and rigid-plastic, incompressible hyperelastic, and hyperelastoplastic J_2 constitutive laws are presented.

5.3.1 Lead extrusion

Bašić *et al.* (2005) calculated the heat generated during axisymmetric forward extrusion of lead using the rigid-plastic without hardening material. The Coulomb’s friction model with maximum coefficient 0.5 is used. The extrusion velocity was 31.5 mm/s and the degree of deformation was 50%. The prescribed initial workpiece temperature was 20°C. The die walls and the free surface are assumed to be adiabatic while on the punch-workpiece contact surface the temperature of 20°C is prescribed. The time step employed was 0.01 s.

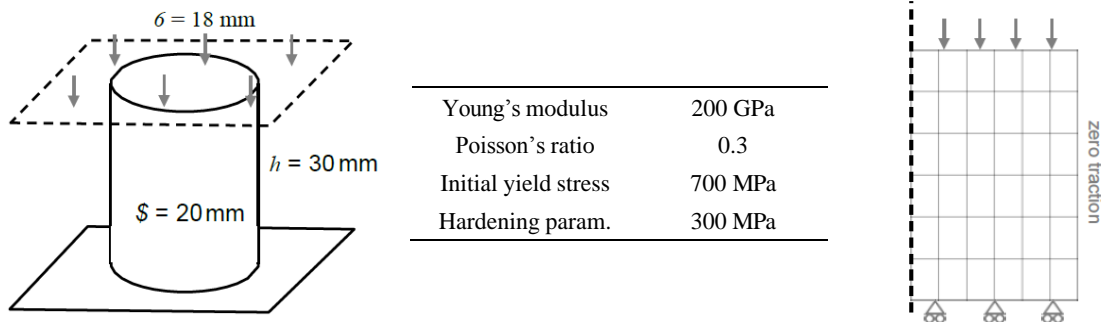


Fig. 20 Upsetting a billet: geometry and loading (left), mechanical properties (middle), and mesh (right) (Cardiff *et al.* 2016b)

The calculated distribution of temperature at $t=1.08\text{ s}$ ($\delta x=34\text{ mm}$) and $t=2.41\text{ s}$ ($\delta x=76\text{ mm}$) are shown in Fig. 18(b) and compared with FEM results of Lippmann (1981) who stated (without a proof) that the experimentally obtained results are generally in agreement with calculations.

5.3.2 Deformation of a rubber cylinder

In this section the FVM is applied to modelling of a large strain problem involving incompressible hyperelastic material. The method is based on the solution of the integral momentum balance equation in total Lagrangian description (Bijelonja *et al.* 2005). An infinitely long homogeneous cylinder with the diameter of 0.4 m made from rubber with Mooney-Rivlin constants $C_1=0.293\text{ MPa}$ and $C_2=0.177\text{ MPa}$ is pressed between two frictionless rigid plates. The problem is considered as the plane strain.

The numerical analysis is performed for two different meshes consisting of 82 and 190 CVs. In Fig. 19 (left) the initial and deformed finite volume meshes were shown. The force-displacement curves for the two meshes are shown in Fig. 19 (right) alongside the finite element results reported in Ansys Verification Manual (2004), where an almost incompressible material is assumed (Poisson's ratio $\nu=0.49967$) and the same Mooney-Rivlin constants as in the FVM calculation are employed. The difference between the finite volume and the finite element simulations is not larger than 2.5%.

5.3.3 Upsetting a billet

The upsetting of a cylindrical billet between parallel rough dies has been analysed by Cardiff *et al.* (2016b). The governing equations are described in updated Lagrangian form and a hyperelasto-plastic J_2 constitutive law is employed. The problem geometry, loading, and material properties are given in Fig. 20. The billet is upset by 60%, corresponding to the die displacement of 18 mm. The contact between the die and billet is rough and is approximated using a penalty method contact procedure with a Coulomb friction coefficient of 0.5. Transient effects are neglected.

The problem is represented as 2D axisymmetric where only the top half of the geometry is modelled. Five separate systematically refined meshes are examined, consisting of 36, 144, 576, 2304 and 9216 quadrilateral cells; the coarsest mesh is shown in Fig. 20(right).

The models have been solved in double precision using 8 CPU cores (2.4 GHz Intel Ivy Bridge cores) in 1000 quasi-static time increments. The required wall-clock time ranged from 15 min for the coarsest mesh to 105 min for the finest mesh.

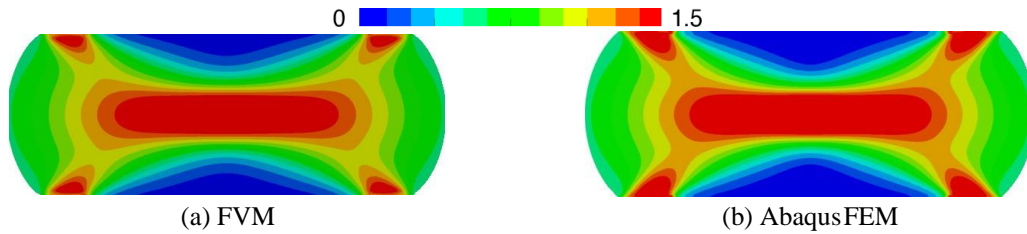


Fig. 21 Upsetting a billet: equivalent plastic strain distribution at 60% upset (Cardiff *et al.* 2016b)

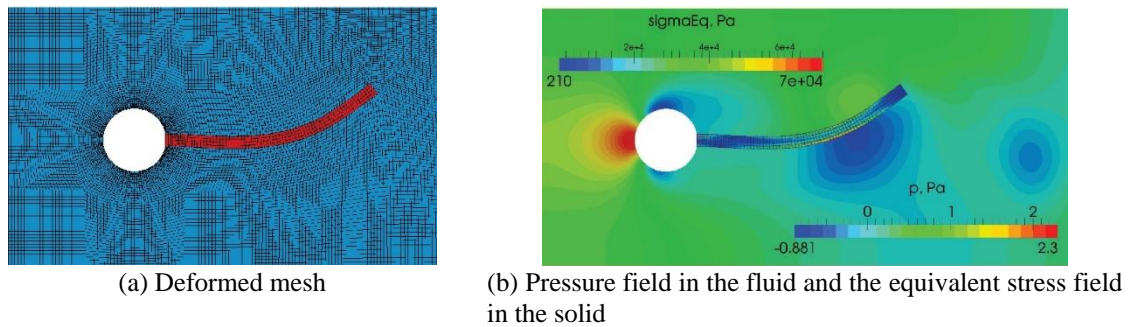


Fig. 22 Elastic plate behind a rigid cylinder: plate tip point at its highest position (Tuković *et al.* 2018)

The predicted equivalent plastic strain distribution at 60% upset is shown in Fig. 21 and compared with the 9 216 cell mesh predictions obtained using commercial FE software Abaqus (version 6.11-1-reduced integration bi-linear quadrilaterals) (Abaqus Theory Manual 2012).

5.4 Fluid-solid interaction

The last few years have shown an increase in methods for multiphysics and, in particular, fluid-solid interaction problems, e.g., Moreno-Navarro *et al.* (2018), Ibrahimbegovic and Boujelben (2018), Hadzalic *et al.* (2018a, b). Since FVMs dominate the fluid flow calculations, the FVM for solid mechanics enables strongly coupled solution procedures, whereby the same discretisation and solution methods are used for both fluid and solid domains. In this section interaction of incompressible Newtonian fluids with elastic plate whose behaviour is modelled by hyperelastic constitutive laws, as well as by Mindlin plate theory.

Tuković *et al.* (2018) considered an elastic plate, 0.35 m long and 0.02 m thick, mounted on a rigid cylinder with a radius of 0.05 m placed in a fluid flow through a horizontal channel of 0.41 m in height and 2.5 m in length. Fluid (density 1000 kg/m^3 , kinematic viscosity $0.001 \text{ m}^2/\text{s}$) enters the channel from the left-hand side with a parabolic velocity profile and average velocity of 1 m/s. A constant pressure at the outlet and a no-slip boundary condition on the walls are imposed. The elastic plate (density 10000 kg/m^3 , Young's modulus $1.4 \times 10^6 \text{ Pa}$, Poisson's ratio 0.4) is described by the Saint Venant-Kirchhoff hyperelastic constitutive model with the plane strain assumption.

Fig. 22(a) shows a section of the discretised spatial domain. The fluid part of the mesh consists of 21,344 and solid part of 328 quadrilateral CVs. The numerical solution is obtained with a time step size of $1.5 \times 10^{-3} \text{ s}$. Fig. 22(b) shows simulation snapshot at the instant of time when the plate tip point is at its highest position. A comparison with the benchmark solutions of Turek and Hron (2006)

Table 6 Elastic plate behind a rigid cylinder: plate tip displacement and force on the plate. The values are given in the same format as in the benchmark paper by Turek and Hron (2006): mean value amplitude [frequency] (Tuković *et al.* 2018)

	Displacement		Force	
	$u_x \times 10^{-3}$ (m)	$u_y \times 10^{-3}$ (m)	F_x (N)	F_y (N)
FVM	-14.26 ± 12.34 [3.9]	1.22 ± 80.2 [1.95]	211.34 ± 75.59 [3.9]	1.23 ± 238.35 [1.95]
<u>Benchmark</u>	-14.58 ± 12.44 [3.8]	1.23 ± 80.6 [2.00]	208.83 ± 73.75 [3.8]	0.88 ± 234.20 [2.00]

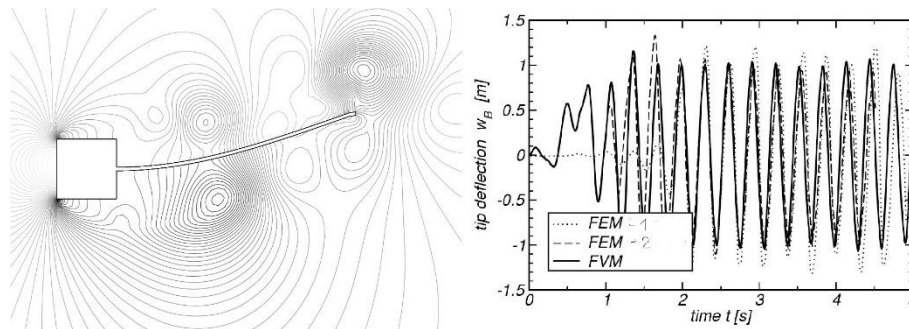


Fig. 23 Elastic plate behind a rigid cylinder: pressure contours around the plate at $t=2$ s (left) and history of the tip deflection (FEM-1 from Wal (1999), FEM-2 from Hübner *et al.* (2001)) (right) (Torlak *et al.* 2002)

is given in Table 6. The difference between the calculated and the benchmark results is around 3% in average for the amplitude and frequency of force and displacement. The relative difference for the mean value of the force y-component goes up to 40%, which can be attributed to the difficulty in calculating the mean value in the case when it is close to zero.

Torlak *et al.* (2002) analysed a thin elastic plate, 4 m long and 0.06 m thick, mounted on a rigid square 1×1 m cylinder placed into a laminar fluid flow with the Reynolds number based on the length of cylinder of 333. The plate is modelled using the Mindlin plate theory. The vortex shedding from the cylinder corners causes plate oscillations which in turn influence the flow significantly, Fig. 23(left).

Comparison of the history of the plate tip displacement with FEM calculations shows a good agreement, Fig. 23(right).

6. Conclusions

It has been established that FV and FE methods start from different governing equations, that they differ in the way they discretise the spatial solution domain and, in particular, in the way they solve the discretised equations.

1. The FVM relies on the first principles only and, in fact, it reduces to the balance of forces acting on a control volume which makes it easy to understand and implement, while the FEM introduces additional concepts, principle of virtual work or the method of weighting residuals, which makes it less appealing to engineers who make the main users community.
2. The FVM discretises space by arbitrary convex polyhedral cells; this enables a discretisation independent of the cell shape and facilitates the automatic numerical mesh generation for the

most complex shapes of solution domain. In the FEM the choice of discretisation elements is limited to a handful of polyhedra, each of which requires different shape functions.

3. The FVM discretisation is second-order accurate and conservative at the local level and consequently for the whole solution domain, whereby the forces acting on the internal cell faces cancel out, and the overall momentum balance reduces to the balance of forces acting on the solution domain boundaries. This feature is at least desirable (makes it reasonably accurate even for very coarse meshes) and in some cases essential. In contrast, the FEM is only globally conservative.

4. Some of the main distinguishing features of the FVM are (a) the unique splitting the stiffness matrix into implicit and explicit parts in a way that generates a very sparsely populated, diagonally dominant coefficient matrix, resulting in extremely low memory requirements and the guaranteed convergence of the efficient iterative solvers and (b) an iterative, inherently nonlinear, segregated solution algorithm, which enables an easy extension of linear to nonlinear problems, with very little additional cost in terms of programming effort, CPU time and memory requirements, as well as an easy coupling of momentum and energy equations, important in many industrial applications. In contrast, the FEM discretisation results in a relatively densely populated stiffness matrix requiring a direct linear algebraic equation solver which additionally fills-up the coefficient matrix; this means that much of the memory needed for problems with large degrees of freedom has to be stored on the disk rather than RAM. While the FVM solution procedure for non-linear problems remains essentially the same as for linear ones, FEMs typically use a full or modified Newton-Raphson loop to resolve nonlinearities.

5. When run in parallel on many processors, the FVM shows practically linear speed-up, enabling a very large, industrial size problems with multi-million degrees of freedom to be solved in an acceptable time. In contrast, a direct linear algebraic equation solver only allows a very modest speed-up of FEMs.

6. The fact that the FVM for solid mechanics uses the same discretisation, data structure and linear algebraic solvers as FVMs for fluid flow calculations enables strongly coupled solution procedures for fluid-solid interaction problems.

However:

7. The standard segregated FVM is not always efficient, especially in cases with strong inter-displacement-component coupling. To remedy this, the geometric multigrid, accelerated convergence, and the block-coupled methods have been proposed.

8. The second-order accuracy of the FVM is not always sufficient (prone to shear-locking). This problem has been addressed by Demirdžić (2016) albeit for discretisation by simple quadrilateral CVs.

9. One indisputable disadvantage of the FVM for solid mechanics, relative to the FEM, is that the field of FV computational solid mechanics is relatively small. This does not, however, take away from the potential of FVM to not only equal but to outperform FE methods for some computational solid mechanics applications; in particular, challenging nonlinear multi-physics problems are seen to be prime candidates.

References

Abaqus 6.11 Theory Manual, Dassault Systèmes Simulia Corp. (2012), http://www.simulia.com/products/abaqus_fea.html.

- Abaqus 6.13 Documentation, Dassault Systèmes Simulia Corp. (2013), <http://dsk.ippt.pan.pl/docs/abaqus/v6.13/index.html>.
- ADINA R & D Inc. (2012), <http://www.adina.com>.
- Ansys-6.1 Verification Manual (2004), http://www oulu.fi/atkk/tkpalv/unix/ansys-6.1/content/Hlp_V_VM201.html.
- Bailey, C. and Cross, M. (1995), "A finite volume procedure to solve elastic solid mechanics problems in three dimensions on an unstructured mesh", *Int. J. Numer. Meth. Eng.*, **38**, 1757-1776. <https://doi.org/10.1002/nme.1620381010>.
- Baliga, B.R. and Patankar, S.V. (1978), "A control-volume based finite element method for convective heat and mass transfer", *2nd International Conference on Computational Methods in Nonlinear Mechanics*, Univ. of Texas, Austin, March.
- Bašić, H., Demirdžić, I. and Muzaferija, S. (2005), "Finite volume method for simulation of extrusion processes", *Int. J. Numer. Meth. Eng.*, **62**, 475-494. <https://doi.org/10.1002/nme.1168>.
- Bathe, K.J. (1996), *Finite Element Procedures*, Prentice Hall, New Jersey.
- Beale, S.B. and Elias, S.R. (1991), "Numerical solution of two-dimensional elasticity problems by means of a SIMPLE-based finite-difference scheme", TR-LT020, National Research Council, Ottawa.
- Bijelonja, I., Demirdžić, I. and Muzaferija, S. (2005), "A finite volume method for large strain analysis of incompressible hyperelastic materials", *Int. J. Numer. Meth. Eng.*, **64**, 1594-1609. <https://doi.org/10.1002/nme.1413>.
- Bijelonja, I., Demirdžić, I. and Muzaferija, S. (2017), "Mixed finite volume method for linear thermoelasticity at all Poisson's ratios", *Numer. Heat Transf. A*, **72**, 215-235. <https://doi.org/10.1080/10407782.2017.1372665>.
- Cardiff, P. and Demirdžić, I. (2018), "Thirty years of the finite volume method for solid mechanics", arXiv:1810.02105v2.
- Cardiff, P., Karač, A. and Ivanković, A. (2012), "Development of a finite volume contact solver based on the penalty method", *Comput. Mater. Sci.*, **64**, 283-284. <https://doi.org/10.1016/j.commatsci.2012.03.011>.
- Cardiff, P., Karač, A. and Ivanković, A. (2014), "A large strain finite volume method for orthotropic bodies with general material orientations", *Comput. Meth. Appl. Mech. Eng.*, **268**, 318-335. <https://doi.org/10.1016/j.cma.2013.09.008>.
- Cardiff, P., Karač, A., De Jaeger, P., Jasak, H., Nagye, J., Ivanković, A. and Tuković, Ž. (2018), "An open-source finite volume toolbox for solid mechanics and fluid-solid interaction simulations", *arXiv preprint arXiv*, 1808.10736.
- Cardiff, P., Tuković, Ž., De Jaeger, P., Clancy, M. and Ivanković, A. (2016), "A Lagrangian cellcentred finite volume method for metal forming simulation", *Int. J. Numer. Meth. Eng.*, **109**, 1777-1803. <https://doi.org/10.1002/nme.5345>.
- Cardiff, P., Tuković, Ž., Jasak, H. and Ivanković, A. (2016), "A block-coupled finite volume method-ology for linear elasticity and unstructured meshes", *Comput. Struct.*, **175**, 100-122. <https://doi.org/10.1016/j.compstruc.2016.07.004>.
- Carolan, D., Tuković, Ž., Murphy, N. and Ivanković, A. (2013), "Arbitrary crack propagation in multi-phase materials using the finite volume method", *Comput. Mater. Sci.*, **69**, 153-159. <https://doi.org/10.1016/j.commatsci.2012.11.049>.
- Clough, R.W. (1960), "The finite element method in plane stress analysis", *Proc. 2nd A.S.C.E. Conf. on Electronic Comp.*, Pittsburgh, PA.
- Das, S., Mathur, S.R. and Murthy, J.Y. (2011), "Unstructured finite-volume method for structure-electrostatic interactions in MEMS", *Numer. Heat Transf. B*, **60**, 425-451. <https://doi.org/10.1080/10407790.2011.628252>.
- Das, S., Mathur, S.R. and Murthy, J.Y. (2012), "Finite-volume method for creep analysis of thin RF MEMS devices using the theory of plates", *Numer. Heat Transf. B*, **61**, 71-90. <https://doi.org/10.1080/10407790.2012.646170>.
- Demirdžić, I. (2008), "Finite volume stress analysis", *STAR-2008 - Computing Technologies of Solving Applied Fluid Dynamics and Stress Analysis Problems*, Nizhny Novgorod.

- Demirdžić, I. (2016), "A fourth-order finite volume method for structural analysis", *Appl. Math. Model.*, **40**, 3104-3114. <https://doi.org/10.1016/j.apm.2015.09.098>.
- Demirdžić, I. and Ivanković, A. (1997), "Finite volume approach to modelling of plates", *Proc. 2nd Congress of Croatian Society of Mechanics*, Brac, Croatia.
- Demirdžić, I. and Martinović, D. (1993), "Finite volume method for thermo-elasto-plastic stress analysis", *Comput. Meth. Appl. Mech. Eng.*, **109**, 331-349. [https://doi.org/10.1016/0045-7825\(93\)90085-C](https://doi.org/10.1016/0045-7825(93)90085-C).
- Demirdžić, I. and Muzaferija, S. (1994), "Finite volume method for stress analysis in complex domains", *Int. J. Numer. Meth. Eng.*, **37**, 3751-3766. <https://doi.org/10.1002/nme.1620372110>.
- Demirdžić, I. and Muzaferija, S. (1995), "Numerical method for coupled fluid flow, heat transfer and stress analysis using unstructured moving meshes with cells of arbitrary topology", *Comput. Meth. Appl. Mech. Eng.*, **125**, 235-255. [https://doi.org/10.1016/0045-7825\(95\)00800-G](https://doi.org/10.1016/0045-7825(95)00800-G).
- Demirdžić, I., Horman, I. and Martinović, D. (2000), "Finite volume analysis of stress and deformation in hygro-thermo-elastic orthotropic body", *Comput. Meth. Appl. Mech. Eng.*, **190**, 1221-1232. [https://doi.org/10.1016/S0045-7822\(99\)00476-4](https://doi.org/10.1016/S0045-7822(99)00476-4).
- Demirdžić, I., Martinović, D. and Ivanković, A. (1988), "Numerical simulation of thermal deformation in welded workpiece", *Zavarivanje*, **31**, 209-219. (in Croatian)
- Demirdžić, I., Muzaferija, S. and Perić, M. (1997), "Benchmark solutions of some structural analysis problems using finite-volume method and multigrid acceleration", *Int. J. Numer. Meth. Eng.*, **40**, 1893-1908. [https://doi.org/10.1002/\(SICI\)1097-0207\(19970530\)40:10<1893:AID-NME146>3.0.CO;2-L](https://doi.org/10.1002/(SICI)1097-0207(19970530)40:10<1893:AID-NME146>3.0.CO;2-L).
- Fainberg, J. and Leister, H.J. (1996), "Finite volume multigrid solver for thermo-elastic stress analysis in anisotropic materials", *Comput. Meth. Appl. Mech. Eng.*, **137**, 167-174. [https://doi.org/10.1016/S0045-7822\(96\)01063-8](https://doi.org/10.1016/S0045-7822(96)01063-8).
- Fallah, N. and Hatami, F. (2006), "A displacement formulation based on finite volume method for analysis of Timoshenko beam", *Proceedings of the 7th International Conference on Civil Engineering*, Tehran, Iran, May.
- Fallah, N. and Parayandeh-Shahrestany, A. (2014), "A novel finite volume based formulation for the elastoplastic analysis of plates", *Thin Wall. Struct.*, **77**, 153-164. <https://doi.org/10.1016/j.tws.2013.09.025>.
- Fryer, Y.D., Bailey, C., Cross, M. and Lai, C.H. (1991), "A control volume procedure for solving the elastic stress-strain equations on an unstructured mesh", *Appl. Math. Model.*, **15**, 639-645. [https://doi.org/10.1016/S0307-904X\(09\)81010-X](https://doi.org/10.1016/S0307-904X(09)81010-X).
- González, I., Naseri, A., Chiva, J., Rigola, J. and Pérez-Segarra, C.D. (2018), "An enhanced finite volume based solver for thermoelastic materials in fluid-structure coupled problems", *6th European Conference on Computational Mechanics (ECCM 6), 7th European Conference on Computational Fluid Dynamics (ECFD 7)*, Glasgow, UK.
- Hadzalic, E., Ibrahimbegovic, A. and Dolarevic, S. (2018), "Fluid-structure interaction system predicting both internal pore pressure and outside hydrodynamic pressure", *Couple. Syst. Mech.*, **7**, 649-668. <https://doi.org/10.12989/CSM.2018.7.6.649>.
- Hadzalic, E., Ibrahimbegovic, A. and Nikolic, M. (2018), "Failure mechanisms in coupled poro-plastic medium", *Couple. Syst. Mech.*, **7**, 43-59. <https://doi.org/10.12989/csm.2018.7.1.043>.
- Hatami, F., Fallah, N. and Pourzeynali, S. (2006), "Application of the finite volume method for shell analysis: A membrane study", Eds. B.H.V. Topping, G. Montero, R. Montenegro, *Proceedings of the Eighth International Conference on Computational Structures Technology*, Civil-Comp Press, Stirlingshire, UK. <https://doi.org/10.4203/csp.83.160>.
- Hübner, B., Walhorb, E. and Dinkler, D. (2001), "Strongly coupled analysis of fluid-structure interaction using space-time finite elements", *European Conference on Computational Mechanics*, Cracow.
- Ibrahimbegovic, A. and Boujelben, A. (2018), "Long-term simulation of wind turbine structure for distributed loading describing long-term wind loads for preliminary design", *Couple. Syst. Mech.*, **7**, 233-254. <https://doi.org/10.12989/csm.2018.7.2.233>.
- Irish Centre for High-End Computing: Abaqus Benchmarks (2013), <https://www.ichec.ie/academic/national-hpc-service/software/abaqus>.
- Isić, S., Doleček, V. and Karabegović, I. (2007), "A comparison between finite element and finite volume methods on the problem of stability of Timoshenko beam", *The 12th International Conference on Problems*

- of *Material Engineering, Mechanics and Design*, Jasna, Slovakia.
- Ivanković, A., Demirdžić, I., Williams, J.G. and Leever, P.S. (1994), "Application of the finite volume method to the analysis of dynamic fracture problems", *Int. J. Fract.*, **66**, 357-371.
- Ivanković, A., Muzaferija, S. and Demirdžić, I. (1997), "Finite volume method and multigrid acceleration in modelling of rapid crack propagation in full-scale pipe test", *Comput. Mech.*, **20**, 46-52. <https://doi.org/10.1007/s004660050215>.
- Jasak, H. and Weller, H. (2000), "Finite volume methodology for contact problems of linear elastic solids", *Proc. of Third International Conference of Croatian Society of Mechanics*, Cavtat/Dubrovnik, Croatia.
- Kanyanta, V., Ivanković, A. and Karač, A. (2009), "Validation of a fluid-structure interaction numerical model for predicting flow transients in arteries", *J. Biomech.*, **42**, 1705-1712. <https://doi.org/10.1016/j.jbiomech.2009.04.023>.
- Lippmann, H. (1981), *Mechanik des Plastischen Fließens*, Springer, Berlin.
- Lou, S., Zhao, G., Wang, R. and Wu, X. (2008), "Modeling of aluminium alloy profile extrusion process using finite volume method", *J. Mater. Proc. Technol.*, **206**, 481-490. <https://doi.org/10.1016/j.jmatprotec.2007.12.084>.
- Martinović, D., Horman, I. and Demirdžić, I. (2001), "Numerical and experimental analysis of wood drying process", *Wood Sci. Technol.*, **35**, 143-156. <https://doi.org/10.1007/s002260000083>.
- Moreno-Navarro, P., Ibrahimbegovic, A. and Perez-Aparicio, J.L. (2018), "Linear elastic mechanical system interacting with coupled thermo-electro-magnetic fields", *Couple. Syst. Mech.*, **7**, 5-25. <https://doi.org/10.12989/csm.2018.7.1.005>.
- National Agency for Finite Element Methods and Standards (1990), *The Standard NAFEMS Benchmarks*, NAFEMS, UK.
- Oñate, E., Cervera, M. and Zienkiewicz, O.C. (1994), "A finite volume format for structural mechanics", *Int. J. Numer. Meth. Eng.*, **37**, 181-201. <https://doi.org/10.1002/nme.1620370202>.
- Perić, M. (2004), "Estimation of iteration errors and convergence speed up", Private Communication.
- Spalding, D.B. (1993), "Simulation of fluid flow, heat transfer and solid deformation simultaneously", *NAFEMS Conference No 4*, Brighton.
- Spalding, D.B. (2006), "Extending the boundaries of heat transfer", *The 13th International Heat Transfer Conference, Sydney, Australia*, August.
- Spalding, D.B. (2008), "Enlarging the frontiers of computational fluid dynamics", *A Lecture at the International Symposium HMT&H in Swirling Flow*, Moscow, October.
- Stylianou, V. and Ivanković, A. (2002a), "Finite volume analysis of dynamic fracture phenomena I. A node release methodology", *Int. J. Fract.*, **113**, 107-123.
- Stylianou, V. and Ivanković, A. (2002b), "Finite volume analysis of dynamic fracture phenomena II. A cohesive zone type methodology", *Int. J. Fract.*, **113**, 125-151.
- Tang, T., Hededal, O. and Cardiff, P. (2015), "On finite volume method implementation of poro-elasto-plasticity soil model", *Int. J. Numer. Anal. Meth. Geomech.*, **39**, 1410-1430. <https://doi.org/10.1002/nag.2361>.
- Taylor, G.A., Bailey, C. and Cross, M. (2003), "A vertex-based finite volume method applied to nonlinear material problems in computational solid mechanics", *Int. J. Numer. Meth. Eng.*, **56**, 507-529. <https://doi.org/10.1002/nme.574>.
- Teskeredžić, A., Demirdžić, I. and Muzaferija, S. (2002), "Numerical method for heat transfer, fluid flow, and stress analysis in phase-change problems", *Numer. Heat Transf. B*, **42**, 437-459. <https://doi.org/10.1080/10407790190054021>.
- Teskeredžić, A., Demirdžić, I. and Muzaferija, S. (2015a), "Numerical method for calculation of complete casting process-Part I: Theory", *Numer. Heat Transf. B*, **48**, 295-316. <https://doi.org/10.1080/10407790.2015.1033296>.
- Teskeredžić, A., Demirdžić, I. and Muzaferija, S. (2015b), "Numerical method for calculation of complete casting process-Part II: Validation and application", *Numer. Heat Transf. B*, **48**, 317-335. <https://doi.org/10.1080/10407790.2015.1033325>.
- Tipton, R. (2017), "A brief history of finite element analysis", <http://nlsde.com/2017/01/04/a-brief-history-of-finite-element-analysis/>.

- Torlak, M., Muzaferija, S. and Perić, M. (2002), "Application of a finite volume method to the computation of interaction between thin linearly elastic structures and incompressible fluid flows", *VDI-Berichte 1862, VDI Tagung Fluid-Struktur-Wechselwirkung*, Wiesloch.
- Tuković, Ž. and Jasak, H. (2007), "Updated Lagrangian finite volume solver for large deformation dynamic response of elastic body", *Tran. FAMENA*, **31**, 55-70.
- Tuković, Ž., Ivanković, A. and Karač, A. (2013), "Finite-volume stress analysis in multi-material linear elastic body", *Int. J. Numer. Meth. Eng.*, **93**, 400-419. <https://doi.org/10.1002/nme.4390>.
- Tuković, Ž., Karač, A., Cardiff, P., Jasak, H. and Ivanković, A. (2018), "OpenFOAM finite volume solver for fluid-solid interaction", *Tran. FAMENA*, **42**, 1-31. <https://doi.org/10.21278/TOF.42301>.
- Turek, S. and Hron, J. (2006), "Proposal for numerical benchmarking of fluid-structure interaction between an elastic object and laminar incompressible flow", Eds. H.J. Bungartz, M. Schäfer, *Fluid-Structure Interaction, Volume 53 of Lecture Notes in Computational Science and Engineering*, Springer, Berlin Heidelberg, 371-385.
- Turner, M.J., Clough, R.W., Martin, H.C. and Topp, L.C. (1956), "Stiffness and deflection analysis of complex structures", *J. Aeronaut. Sci.*, **23**, 805-823.
- Voler, V.R. (2009), *Basic Control Volume Finite Element Methods for Fluids and Solids*, World Scientific Publishing Co. Pte. Ltd., London.
- Wal, W. (1999), "Fluid-Struktur-Interaktionen mit stabilisierten Finiten Elementen", Bericht Nr. 31, Institut für Baustatik der Universität Stuttgart.
- Zienkiewicz, O.C. and Oñate, E. (1991), "Finite volumes vs finite elements. Is there really a choice?", Eds. P. Wriggers, W. Wagner, *Nonlinear Computational Mechanics. State of the Art*, Springer, Berlin.
- Zienkiewicz, O.C., Taylor, R.L. and Nithiarasu, P. (1967), *The Finite Element Method for Fluid Dynamics*, McGraw-Hill.